

Jean-François Bérar*, Nathalie Boudet, Nils Blanc, and Shinya Hosokawa

Resonant Scattering in Condensed Matter, Experiments that Reveal Short to Long Range Atomic Order

DOI 10.1515/zpch-2015-0699

Received October 12, 2015; accepted November 24, 2015

Abstract: After a historical introduction of the anomalous dispersion effect, the formalism used to investigate disordered materials using the resonant scattering of X-rays is exposed. As these experiments are sensitive to the experimental conditions, some experimental settings are discussed.

Keywords: Anomalous Scattering, Condensed Matter.

1 Introduction

The story of anomalous scattering started from the evidence of light dispersion using prism by Newton in 1665. Studying dispersion of iodine vapor, Leroux [1] remarked the refraction behaved “anomalously” as it decreased instead of increasing. Evidence of such an effect in magenta alcoholic solution by Christiansen [2], allowed Kundt [3] to make the link with absorption edges. A few years after, Hurion [4] proved that the anomalous effect did not depend on the experimental procedure and compared known experimental results with theoretical ones.

A few years after the X-ray discovery by Roentgen [5], Laue evidenced their diffraction by crystals [6] then Friedel [7] stated that X-ray diffraction is not able to reveal the lack of a symmetry center, a general property of Fourier transformations for real functions, as far as there is no X-ray dichroism.

*Corresponding author: Jean-François Bérar, Institut Néel, CNRS, Grenoble, France, e-mail: jean-francois.berar@neel.cnrs.fr

Nathalie Boudet, Nils Blanc: Institut Néel, CNRS; and Université Grenoble Alpes, F38000 Grenoble, France

Shinya Hosokawa: Department of Physics, Kumamoto University, Kumamoto, Japan

In 1919, Stenström [8] reported dispersion from the Bragg's law which can be interpreted as a refraction effect but the discovery of X-ray anomalous dispersion has been done by Larsson, Siegbahn and Waller [9] in 1924 by refraction measurements. Then Kronig [10] published in 1926 the theory of the dispersion of X-rays whose basic relations were derived independently by Kramers [11]. A few years after, Kronig [12] published the EXAFS interpretation.

First applications of X-ray anomalous scattering were reported in the 1930's. They concerned materials studies. It is only in 1949 that Bijvoet [13] showed how anomalous scattering allows to distinguish between $F(hkl)$ and $F(\bar{h}\bar{k}\bar{l})$ and then to solve the absolute configuration problem of crystals, opening the first large application field of the anomalous scattering.

But anomalous scattering became only widely used with the availability of X-ray synchrotron sources as they allow to adjust continuously the energy of the incoming beam, energies near absorption edges can then be selected: below the edge the real part of the scattering factor decreases strongly, whereas above, its imaginary part rises up.

However, the real use of anomalous scattering started with X-ray dedicated synchrotron sources as illustrated by dedicated meetings (Malente, Germany (1992), Aussois, France (2011) [14], Oxford, Great Britain (2013) [15]). A review of diffraction applications has been published in [21]. Let us recall the following.

In macromolecules crystallography [16], most diffraction studies start by anomalous scattering experiments to be able to know the phase of the reflexions and therefore to solve the structure.

As low energy edges can enhance the magnetic scattering sensitivity by some hundred, resonant scattering experiments became an important tool in studies of magnetism [17]. The tensorial properties of the resonant scattering has allowed a new range of crystallographic studies exploring the so called forbidden reflexions [18].

One of the most important contribution of anomalous scattering is the possibility to perform simultaneously spectroscopic and crystallographic experiments. This allows Diffraction Anomalous Fine Structure, DAFS, experiments to access to the structure of nanomaterials [19, 20]: scattering intensities collected at different edges are characteristic of the structure around each species.

2 X-ray anomalous or resonant scattering

In simple cases, the scattering power of X-rays by an atom can be expressed by means of its scattering factor f which depends not only on the scattering vector

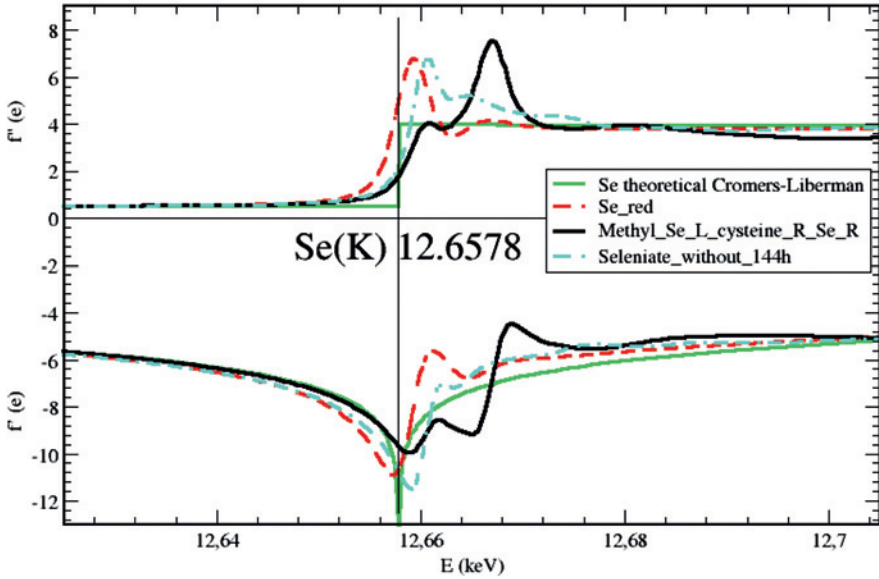
Se (Z=34) f' , f'' anomalous factors

Figure 1: Theoretical Se edge compared to the experimental ones on Se found in selenates, one can notice a chemical shift, an important white line and “ripples” known as EXAFS oscillations. Edges were recorded on CRG FAME beamline at ESRF and calculated f' .

Q but also on the scattering energy E :

$$f(Q, E) = f_o(Q) + f'(E) + if''(E)$$

Both f' and f'' are known as the anomalous scattering factors. They are linked to the optical characteristic values, the refractive index n and the absorption coefficient μ by:

$$n(E) = 1 - 2\pi e^2 \hbar^2 / mE^2 - \sum_a N_a f'_a(E) = 1 - \varepsilon \text{ with } \varepsilon \approx 10^{-6}$$

$$\mu(E) = (4\pi \hbar e^2 / mcE) \sum_a N_a f''_a(E)$$

Then f' and f'' are linked to each other through the Kramers–Kronig relations

$$f'(E) = 2/\pi \int_0^\infty \frac{E' f''(E')}{(E^2 - E'^2)} dE' \quad (1)$$

$$f''(E) \propto \int_0^\infty \frac{E' f'(E')}{(E^2 - E'^2)} dE' \quad (2)$$

This allows to calculate f' values near the edges, where the tabulated values are not always accurate enough, as shown on Figure 1. They depend on the experimental setting and the selected atom in the material. Shortly, if the energy chosen in the experiment is far from the edge energy E , i.e. if $\Delta E/E$ is bigger than 5‰ tabulated values can be used. If the relative difference is lower than 1‰ experimental values have to be used. In between these values, one can often use the tabulated values but after shifting the experimental values to match the energy position of the tabulated edge.

Anomalous scattering plays an important role in investigating complex structures: it helped to elucidate the first atomic structure of a quasicrystal [22]; it allows to investigate diffusion in multi layers [23]. Anomalous scattering has been used in powder crystallography to solve problems related to substitution, for examples, it has allowed to assess the $\text{Fe}^{2+}/\text{Fe}^{3+}$ ratio on both sites tetra and octa of Ferrite depending on the temperature [24] as well as Sr/Rb in complex X-zeolite [25].

Hereafter, we will be concerned by the case of amorphous materials or liquids where anomalous scattering is a major way in their experimental study.

The scattered intensity in suitable dimensionless units may be written generally as, α and β being the atomic species and n_α and m_β the respective atoms:

$$I(\mathbf{Q}) = \sum_{\alpha} f_{\alpha}(\mathbf{Q}) \sum_{n_{\alpha}} e^{i\mathbf{Q}\mathbf{r}_{n_{\alpha}}} \sum_{\beta} f_{\beta}(\mathbf{Q}) \sum_{m_{\beta}} e^{-i\mathbf{Q}\mathbf{r}_{m_{\beta}}}$$

$$I(\mathbf{Q}) = \sum_{\alpha} \sum_{\beta} f_{\alpha}(\mathbf{Q}) f_{\beta}(\mathbf{Q}) \left(N_{\alpha\beta} + \sum_{n_{\alpha}} \sum_{m_{\beta} \neq n_{\alpha}} e^{i\mathbf{Q}(\mathbf{r}_{n_{\alpha}} - \mathbf{r}_{m_{\beta}})} \right)$$

In disordered materials, it is convenient to replace the sum over $m = n$ by a continuous integral and, as X-ray scattering arises from deviation in electron density from its average, to add and subtract a term proportional to the average atomic density. Then using the partial functions $g_{\alpha\beta}(\mathbf{r})$, the intensity can be rewritten as, with x_{α} and x_{β} being the atomic concentrations and ρ_o the atomic density:

$$I(\mathbf{Q}) = \sum_{\alpha} \sum_{\beta} f_{\alpha}(\mathbf{Q}) f_{\beta}(\mathbf{Q}) N_{\alpha\beta} \left(1 + \rho_o x_{\alpha} x_{\beta} \int_V [g_{\alpha\beta}(\mathbf{r}) - 1] e^{i\mathbf{Q}\mathbf{r}} dV \right)$$

$$+ \rho_o \sum_{\alpha} \sum_{\beta} f_{\alpha}(\mathbf{Q}) f_{\beta}(\mathbf{Q}) N_{\alpha\beta} \int_V x_{\alpha} x_{\beta} e^{i\mathbf{Q}\mathbf{r}} dV$$

The upper line corresponds to scattering associated to short range order $I^{SRO}(\mathbf{Q})$ whereas the lower line is associated with the intensity scattered at small

angle $I^{\text{SAXS}}(\mathbf{Q})$. Introducing the partial structure factors $S_{\alpha\beta}(\mathbf{Q})$ gives:

$$I^{\text{SRO}}(\mathbf{Q}) = \sum_{\alpha} \sum_{\beta} f_{\alpha}(\mathbf{Q}) f_{\beta}(\mathbf{Q}) N_{\alpha\beta} \left(1 + \rho_o x_{\alpha} x_{\beta} \int_0^{\infty} 4\pi r^2 [g_{\alpha\beta}(r) - 1] \frac{\sin(\mathbf{Q}r)}{\mathbf{Q}r} dr \right)$$

$$I^{\text{SRO}}(\mathbf{Q}) = \sum_{\alpha} \sum_{\beta} f_{\alpha}(\mathbf{Q}) f_{\beta}(\mathbf{Q}) N_{\alpha\beta} S_{\alpha\beta}(\mathbf{Q})$$

$$S_{\alpha\beta}(\mathbf{Q}) = 1 + \frac{4\pi\rho_o}{\mathbf{Q}} x_{\alpha} x_{\beta} \int_0^{\infty} [g_{\alpha\beta}(r) - 1] r \sin(\mathbf{Q}r) dr$$

In an anomalous experiment performed at two energies $E_{\gamma f}$ far from the edge, and $E_{\gamma n}$ close to the absorption edge of the γ atom, the difference $\Delta_{\gamma} I^{\text{SRO}}(\mathbf{Q})$ between the two values of $I^{\text{SRO}}(\mathbf{Q})$ becomes assuming that only f_{γ} varies from Δf_{γ} :

$$\Delta_{\gamma} I^{\text{SRO}}(\mathbf{Q}) = \sum_{\alpha} \sum_{\beta} (f_{\alpha}(\mathbf{Q}, E_{\gamma n}) f_{\beta}(\mathbf{Q}, E_{\gamma n}) - f_{\alpha}(\mathbf{Q}, E_{\gamma f}) f_{\beta}(\mathbf{Q}, E_{\gamma f})) N_{\alpha\beta} S_{\alpha\beta}(\mathbf{Q})$$

$$\Delta_{\gamma} I^{\text{SRO}}(\mathbf{Q}) = \sum_{\alpha} \sum_{\beta} ((f_{\alpha}(\mathbf{Q}) + \Delta f_{\alpha}(\mathbf{Q})) (f_{\beta}(\mathbf{Q}) + \Delta f_{\beta}(\mathbf{Q})) - f_{\alpha}(\mathbf{Q}) f_{\beta}(\mathbf{Q}))$$

$$\times N_{\alpha\beta} S_{\alpha\beta}(\mathbf{Q})$$

$$\Delta_{\gamma} I^{\text{SRO}}(\mathbf{Q}) = \Delta f_{\gamma}^2(\mathbf{Q}) N_{\gamma\gamma} S_{\gamma\gamma}(\mathbf{Q}) + 2\Delta f_{\gamma}(\mathbf{Q}) \sum_{\beta} f_{\beta}(\mathbf{Q}) N_{\gamma\beta} S_{\gamma\beta}(\mathbf{Q})$$

$$\Delta_{\gamma} I^{\text{SRO}}(\mathbf{Q}) \approx 2\Delta f_{\gamma}(\mathbf{Q}) \sum_{\beta} f_{\beta}(\mathbf{Q}) N_{\gamma\beta} S_{\gamma\beta}(\mathbf{Q})$$

From the last relations, it is obvious that $\Delta_{\gamma} I^{\text{SRO}}(\mathbf{Q})$ enhances the contribution of the γ atom, given a weighted sum of the density function around it.

Different formalisms as e.g. Faber–Ziman [26], Ashcroft–Langreth [27], ... allow to define radial density functions. The Faber–Ziman method which was developed for neutrons studies, has been extended to liquid alloys of transition metals [28]. With the availability of X-rays produced by synchrotron, this formalism has been extended to amorphous compounds such as semiconducting [29] and metallic [30] glasses.

Using the Faber–Ziman method, the contrast $\Delta_{\gamma} I^{\text{SRO}}(\mathbf{Q})$ and the partial structure factors $S_{\alpha\beta}^{\text{FZ}}(\mathbf{Q})$ are expressed as:

$$k_{\gamma} \Delta_{\gamma} I^{\text{SRO}}(\mathbf{Q}) = \Delta_{\gamma} [\langle f^2 \rangle - \langle f \rangle^2] + \Delta_{\gamma} [\langle f \rangle^2] \Delta_{\gamma} S(\mathbf{Q})$$

$$\Delta_{\gamma} S(\mathbf{Q}) = \sum_{\alpha} \sum_{\beta} W_{\alpha\beta}(\mathbf{Q}, E_{\gamma}) S_{\alpha\beta}^{\text{FZ}}(\mathbf{Q})$$

$$W_{\alpha\beta}(\mathbf{Q}, E_{\gamma}) = x_{\alpha} x_{\beta} \frac{\Delta_{\gamma} [f_{\alpha} f_{\beta}]}{\Delta_{\gamma} [\langle f^2 \rangle]}$$

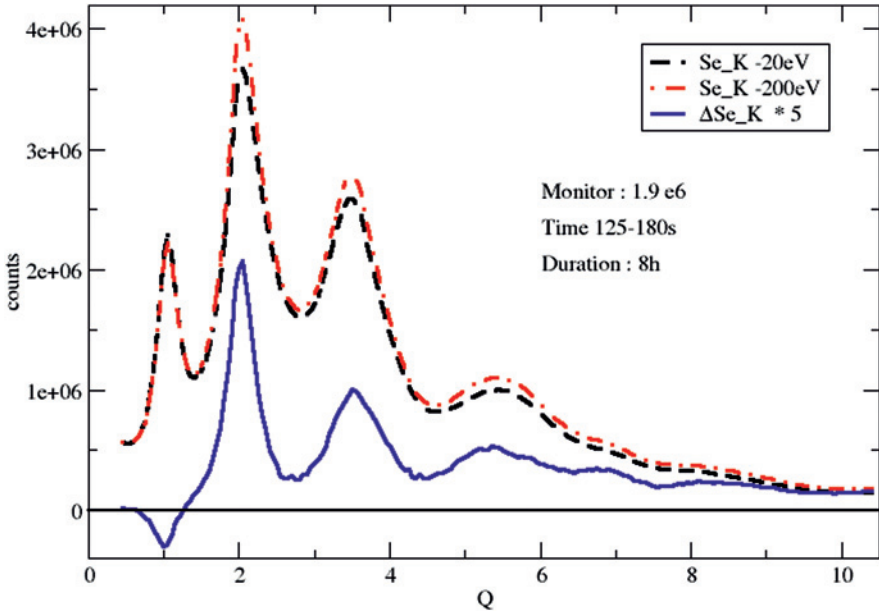


Figure 2: Due to the weakness of the measured signal, it is mandatory to obtain reliable difference between very near and near edge measurements. Raw data recorded with 60 eV resolution on the CRG D2AM beamline at ESRF in April 2014.

in which $\Delta_\gamma[\dots]$ indicates the difference of values in the bracket at the energies of E_{γ_f} and E_{γ_m} , close to the absorption edge of the γ -th element, and $\langle \rangle$ represents the chemical average of the atomic form factors; $W_{\alpha\beta}(Q, E_\gamma)$ takes only significant values when α or β is γ .

It should be noted that compared to $S(Q)$, $\Delta_\gamma S(Q)$ highly enhances the partial contributions from the γ -th element, and suppresses the other partials, an example is reported in Figure 2.

However, to obtain significant values, fluorescence and Compton contributions, visible on Figure 3 have to be removed from experimental data. Using suitable experimental settings [31] these contributions were estimated from energy scans at constant Q to be less than 0.2% along the whole experimental Q range. Moreover, subtracting the two scattering functions at near- and far-edge incident energies, this reduced the spurious Compton contribution even at high Q values down to less than 0.005%. To reach the needed good signal to noise ratio, more than three million counts were acquired at the $S(Q)$ maximum, which typically takes less than six hours per scan.

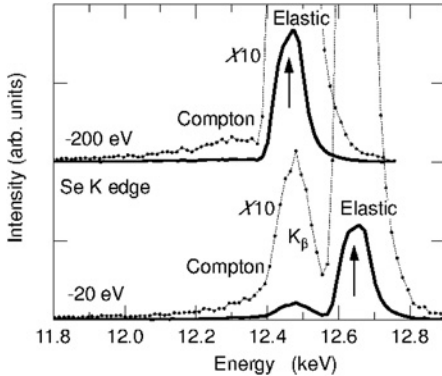


Figure 3: Experimental energy scan near and far from Se_K edge.

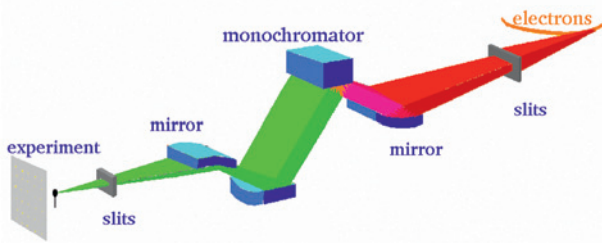


Figure 4: Schematic diagram of the optics used for experiments on CRG-D2AM beamline at ESRF. This setting uses either Si(111) or Si(311).

3 Experimental settings

All the experiments using anomalous scattering depend strongly on the experimental settings. In the following, the energy resolution compared to the counting range of some of them, used for recording the differential structure factors of amorphous materials, is discussed.

The following setting (Figure 4) is used on the CRG D2AM beamline at ESRF, noted as D2AM hereafter, to ensure the needed characteristics for the incoming beam: energy continuously tunable between 5 and 30 keV with an energy resolution $\Delta E/E$ better than 1×10^{-4} and an energy stability $\Delta E/E$ better than 5×10^{-5} .

X-rays generated by a bending magnet source are monochromatized using a Si(111) double-crystal monochromator with a sagittal focussing system for the second crystal. Si(311) or Si(220), can also be used depending on the edge. The monochromator is located between two cylindrically bent mirrors made of Si coated with Pt. This X-ray optics provides a small incident X-ray beam of 0.1 mm in height and 0.3 mm in width, and an energy resolution of about 1 eV at an incident X-ray energy near 10 keV. The diffraction experiments are performed using a standard $\omega-2\theta$ diffractometer at two energies (typically 20 or 30 eV, and 200 eV)

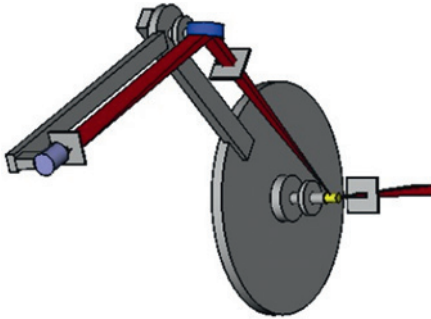


Figure 5: Schematic drawing of the setting used with flat analyser, the horizontal size of the beam on the receiving slits is twice its size on the analyzer crystal.

below the K edge of each element. The energy of the incident X-ray beam is calibrated using the absorption edges of samples during the experiments.

For the detection system, some choices are open:

- The classical powder settings which use high quality analyser crystals; the analyser resolution removes fluorescence but its acceptance is too limited and this setting seems not suited for amorphous compounds as the count rate is too weak, typically some thousandth of the two following settings.
- The use of detectors with electronic windows has been considered but their energy resolution is too weak, typically for a X-ray Si(Li) ΔE is bigger than 150 (250) eV at Se_K edge. Even if important improvements have been made, they have concerned mainly the size of the active surface and the counting capacity. The resolution of solid state detectors is limited intrinsically by the statistics of the generated charge carriers, a Fano modified Poisson distribution [32] and by noise and non-uniformities in charge collection efficiency. With such an energy resolution, the data correction needed to remove fluorescence and Compton contribution becomes important and takes long time to ensure the correctness of the resulting data.
- Focussed beam used together with pyrolytic carbon analyzer (mosaicity ≈ 0.4 deg), Figure 5. This setting seemed to be a valuable choice and it has been used up to 2005 on the D2AM beamline. An energy resolution $\Delta E \approx 50$ eV was obtained using a common distance d_A between sample-crystal D_{SC} and crystal-analyser slits D_{CA} slits of 500 mm with a beam height at sample position δ_S of 100 μm and analyser slits height δ_A of 400 μm the angular resolution being $\Delta 2\theta \approx 0.4$ deg. For a horizontally focussed beam, the parafocussing error depends mainly on the horizontal aperture of the slits L_A .

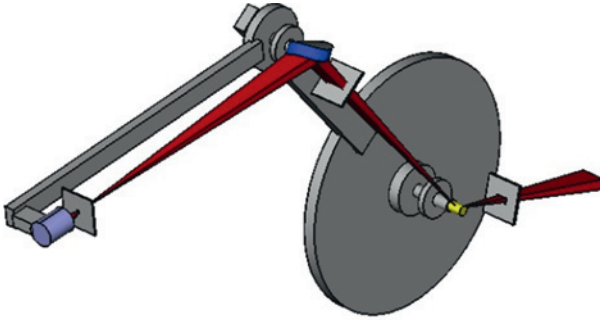


Figure 6: Schematic drawing of the setting used with curved analyser allowing transverse focussing.

$$\text{Energy resolution} : \Delta E/E = (\delta_S + \delta_A)/2d_A \tan \theta_A$$

$$\text{Parafocussing error} : \Delta E/E = \left(\frac{1}{D_{SC}} - \frac{1}{D_{CA}} \right) \frac{L_A \cos \theta_A}{2}$$

The main limitations of this setting were the weakness of measured flux, which was limited by the horizontal aperture defined by the crystal size and by the width of the receiving slits.

- Vertically focussed beam used with a sagittally curved pyrolytic carbon analyzer: this setting, Figure 6 has improved the previous one removing its limit. The scattered beam was focussed horizontally on the receiving slits, this had allowed to use wider analyzer. Crystals with a width of 40 mm were used on the D2AM beamline since 2005.

The energy resolution remained the same but the collection efficiency was improved by the gain due to transverse focalisation. Two crystals with different radius allowed to cover the energy range from 10 keV to 30 keV: the value of sagittal radius $R_T = d_A \sin \theta_A$ was not critical, leading only to an horizontal enlargement of the spot.

- 1D vertical detector associated with a sagittally curved pyrolytic carbon analyzer, can be used. The graphite mosaicity (≈ 0.4 deg) allows a direct measurement of energy profile avoiding to rescan it as a function of \mathbf{Q} , but as the energy scan occurs in the same direction as the \mathbf{Q} scan, slits will be needed before the crystal analyzer.
- 2D detector associated with a curved pyrolytic carbon analyzer, can be used to improve the collection efficiency. In this case, the crystal analyzer will be set in order to deviate the scattered beam in the transverse plane, Figure 7. Compared to the setting used on D2AM, the deviation will be affected by a small polarization loss (≈ 0.9) but several steps in \mathbf{Q} can be measured at each detector position: receiving slits being no more needed as the resolution is given by the pixel size (typically 100–200 μm). Moreover, due to the graphite mosaicity

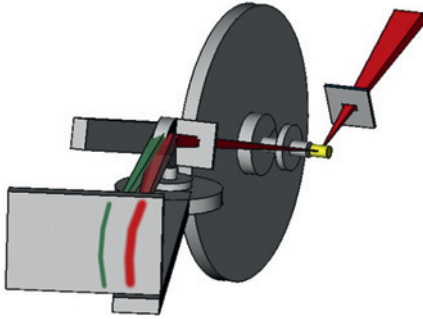


Figure 7: Schematic drawing of the setting proposed with curved analyser combined with 2D detector. The 2D data drawn on the detector are scattering and fluorescence signals.

ity a direct measurement of energy profile will be measured in the transverse plane for each step. This setting, which will soon be tested on the D2AM beam-line, will allow to collect a lower number of steps or to count a lower time at each position.

Another advantage of the detecting system based on pyrolytic carbon analyzer, is the simpler data analysis compared to SSD setting. Typically, it had taken less than a half day to extract the final $\Delta_i S(Q)$ functions out of the raw scattering data. For a similar experiment on As_2Se_3 glass [20] where a SSD detector was used, the data analysis took more than two weeks, mainly to correct for the fluorescent X-ray contributions.

4 Conclusion

The study of glasses and other amorphous materials using anomalous scattering has reached a mature state as the needed experimental data can now be obtained with the required quality on synchrotron sources within a reasonable experimental time. Numerous results obtained can be compared with numerical ones deduced from molecular dynamics.

References

1. F. P. Leroux, C. R. Acad. Sc. **55** (1862) 126.
2. C. Christiansen, Pogg. Ann. **141** (1870) 479.
3. A. Kundt, Ann. Phys. **219** (1871) 149, DOI:10.1002/andp.18712190513.

4. A. Hurion, *Ann. Sci. Ecole. Norm. S.* **6** (1877) 367, http://www.numdam.org/item?id=ASENS_1877_2_6_367_0.
5. W. Röntgen, *Über eine neue Art von Strahlen*, aus den Sitzungsberichten der Würzburger Physik.-medic. Gesellschaft (1895).
6. M. von Laue, *Phys. Z.* **14** (1913) 1075.
7. G. Friedel, *C. R. Acad. Sc.* **157** (1913) 1533.
8. W. Strenström, Dissertation, Lund (1919).
9. A. Larsson, M. Siegbahn, and I. Waller, *Naturwiss.* **52** (1924) 1212.
10. R. de L. Kronig, *J. Opt. Soc. Am.* **12** (1926) 547, DOI:10.1364/JOSA.12.000547.
11. H. A. Kramers, *Atti Cong. Intern. Fisici*, (Transactions of Volta Centenary Congress) Como 2 (1927) 545.
12. R. de L. Kronig and H. A. Kramers, *Z. Phys.* **48** (1928) 174.
13. J. M. Bijvoet, *Proc. K. Ned. Akad. Wet. B*, **52** (1949) 313.
14. Internat. School/Conf. on Resonant Elastic X-Ray Scattering in Condensed Matter, 2011 Aussois (France), *Eur. Phys. J.-Spec. Top.* **208** (2012) (special issue).
15. REXS 2013 – Workshop on Resonant Elastic X-ray Scattering in Condensed Matter, 2013 Oxford (UK), *J. Phys. Conf. Ser.* **519** (2013) (special issue).
16. R. Kahn, E. Girard, and R. Fourme, *Eur. Phys. J.-Spec. Top.* **208** (2012) 15.
17. C. Vettier, *J. Magn. Mater.* **129** (1994) 59.
18. J. Kokubun and V. E. Dmitrienko, *Eur. Phys. J.-Spec. Top.* **208** (2012) 39.
19. H. Renevier and M. G. Proietti, Grazing Incidence Diffraction Anomalous Fine Structure in the Study of Structural Properties of Nanostructures, in: *Characterization of Semiconductor Heterostructures and Nanostructures*, C. Lamberti, G. Agostini (Eds.), Elsevier, Amsterdam (2013).
20. V. Favre-Nicolin, M. G. Proietti, C. Leclere, N. A. Katcho, M.-I. Richard, and H. Renevier, *Eur. Phys. J.-Spec. Top.* **208** (2012) 189.
21. J. L. Hodeau, V. Favre-Nicolin, S. Bos, H. Renevier, E. Lorenzo, J. F. Berar, *Chem. Rev.*, **101** (2001) 1843.
22. H. Takakura, C. Gómez, A. Yamamoto, M. De Boissieu, and A. Tsai, *Nat. Mater.* **6** (2007) 58, DOI:10.1038/nmat1799.
23. U. Staub, H. Grimmerd, and H.-Ch. Mertins, *J. Phys.-Condens. Mat.* **11** (1999) 5691, DOI:10.1088/0953-8984/11/30/301.
24. F. Bernard, J. Lorimier, V. Nivoix, N. Millot, P. Perriat, B. Gillot, J.-F. Berar, and J. C. Niepce, *J. Solid State Chem.* **141** (1998) 105.
25. H. Palancher, J.-L. Hodeau, C. Pichon, J.-F. Berar, J. Lynch, B. Rebours, and J. Rodriguez-Carvajal, *Angew. Chem. Int. Edit.* **44** (2005) 1725.
26. T. E. Faber and J. M. Ziman, *Phil. Mag.* **11** (1965) 153.
27. N. W. Ashcroft and D. C. Langreth, *Phys. Rev.* **166** (1968) 934.
28. R. Evans, H.-J. Güntherodt, H. U. Künzi, and A. Zimmermann, *Phys. Lett. A*, **38** (1972) 151.
29. P. H. Fuoss, W. K. Warburton, A. Bienentock, and P. Eisenberger, *Phys. Rev. Lett.* **46** (1981) 1537.
30. J. C. de Lima, J. M. Tonnerre, and D. Raoux, *J. Non-Cryst. Solids* **106** (1988) 38.
31. S. Hosokawa, W.-C. Pilgrim, J.-F. Berar, and S. Kohara, *Eur. Phys. J.-Spec. Top.* **208** (2012) 291.
32. U. Fano, *Phys. Rev.* **72** (1947) 26.